Humic-like acids from hydrochars: Study of the metal complexation properties compared with humic acids from anthropogenic soils using PARAFAC and time-resolved fluorescence

João Vitor do Santos[a], Lais Gomes Fregolente[a,b], Altair Benedito Moreira[a], Odair Pastor Ferreira[b], Stéphane Mounier[c], Bruno Viguier[c], Houssam Hajjoul[c], and Márcia Cristina Bisinoti[a*]

[a] Laboratório de Estudos em Ciências Ambientais, Departamento de Química e Ciências Ambientais, Instituto de Biociências, Letras e Ciências Exatas, Universidade Estadual Paulista "Júlio de Mesquita Filho," 15054-000, São José do Rio Preto, São Paulo, Brazil.

[b] Laboratório de Materiais Funcionais Avançados (LaMFA), Departamento de Física, Universidade Federal do Ceará, 60455-900, Fortaleza, Ceará, Brazil.

[c] Laboratoire MIO–Equipe CEM, Université de Toulon, CS 60584, 83041, CEDEX 9, Toulon, France.

[*]Corresponding author

Name: Márcia Cristina Bisinoti

E-mail: marcia.bisinoti@unesp.br

Phone: +55 17 3221-2352

Address: Laboratório de Estudos em Ciências Ambientais, Departamento de Química e Ciências Ambientais, Instituto de Biociências, Letras e Ciências Exatas, Universidade Estadual Paulista "Júlio de Mesquita Filho", Rua Cristóvão Colombo, 2265, 15054-000, São José do Rio Preto, São Paulo State, Brazil.

Abstract

Humic acids (HA) play an important role in the distribution, toxicity, and bioavailability of metals in the environment. Humic-like acids (HLA) that simulate geochemical processes can be prepared by NaOH aqueous extraction from hydrochars produced by hydrothermal carbonization (HTC). HLA can exhibit properties such as those found in HA from soils, which are known for their ability to interact with inorganic and organic compounds. The molecular characteristics of HLA and HA help to explain the relationship between their molecular features and their interaction with metallic species. The aim of this study is to assess the molecular features of HA extracted from *Terra Mulata* (TM) and HLA from hydrochars as well as their interaction with metals by using Cu(II) ions as a model. The results from ^{13}C NMR, elemental analysis, FTIR, and UV-Vis showed that HA are composed mostly of aromatic structures and oxygenated functional groups, whereas HLA showed a mutual contribution of aromatic and aliphatic structures as main constituents. The interactions of HA and HLA with Cu(II) ions were evaluated through fluorescence quenching, in which the density of complexing sites per gram of carbon for interaction was higher for HLA than for HA. Furthermore, the HLA showed similar values for stability constants, and higher than those found for other types of HA in the literature. In addition, the average lifetime in both humic extracts appeared to be independent of the copper addition, indicating that the main mechanism of interaction was static quenching with a non-fluorescent ground-state complex formation. Therefore, the HLA showed the ability to interact with Cu(II) ions, which suggests that their application can provide a new approach for remediation of contaminated areas.

Keywords: hydrothermal carbonization, anthropogenic soils, complexation, fluorescence lifetime, soil remediation

1. Introduction

Metal pollution is a worldwide environmental issue in which human activity plays a major role (Lesmana et al., 2009; Li et al., 2014). Unlike most organic contaminants, metals are not biodegradable and can accumulate in living organisms, thereby causing problems for both human health and the environment (Lesmana et al., 2009). Some metals of great concern are cadmium, zinc, copper, and nickel (Li et al., 2014; Tang et al., 2014). Among them, copper is important for cellular metabolism. However, this element is highly toxic if swallowed at high concentrations and can cause gastrointestinal problems, hair loss, weight loss, and even death (Andreazza et al., 2010; Fu and Wang, 2011; Tang et al., 2014). Intensified industrial, agricultural, mining, and urbanization activities are the main causes of copper contamination (Hladun et al., 2015; MacKie et al., 2012). Therefore, research is needed to develop techniques for reducing the concentrations of metals in contaminated soils.

It is widely accepted that soil fertility depends on the presence of nutrients and organic matter (Stevenson, 1994). Humic substances (HS) are the main constituents of soil organic matter and are formed from the remains of plant and animal degradation. Humic acids (HA) are one of the components of HS. They represent the most hydrophobic part and play important roles in soil fertility, water retention, plant growth promotion, and interaction with organic and inorganic compounds (Bento et al., 2019; Canellas and Façanha, 2004; Jindo et al., 2016). The bioavailability, distribution, and toxicity of pollutants are affected by their interaction (He et al., 2016; Tang et al., 2014); thus, the use of HA has gained attention for remediation (Piccolo et al., 2019).

Anthropogenic soils such as TM occur near the Amazon basin and are known for exhibiting high fertility (Glaser et al., 2000; Oliveira et al., 2018). Such soils have gained the attention of researchers who have attempted to reproduce their organic matter

by thermochemical methods of biomass conversion, such as pyrolysis and hydrothermal carbonization (HTC). These methods use various biomass types to obtain a material with the characteristics of TM.

The HTC process is a suitable biomass disposal method for the production of carbon-based materials known as hydrochar. In addition, the process water (liquid phase) is generated by this method. Some authors have proposed the use of this process water as a hydrothermal medium in a new carbonization process (Kabadayi Catalkopru et al., 2017; Stemann et al., 2013; Weiner et al., 2014) or for liquid fertilizer (Fregolente et al., 2018).

Most HA used in the literature are extracted from soils, water, sediments, or peat (Chen et al., 2015; Plaza et al., 2005; Zherebtsov et al., 2015). The formation of these environmental elements under natural conditions requires significant amounts of time and involves several chemical and biological reactions that can last for years (Yang et al., 2019a). However, the formation of HTC needs only hours (Melo et al., 2017; Silva et al., 2017). Humic-like acids (HLA) are defined as extracts of different organic materials that have not undergone the natural process of humification (Bento et al., 2019; Jindo et al., 2016, 2019). Although there is not the natural humification process that occurs in soils, HLA extracted from hydrochars might have characteristics similar to those of natural HA extracted from anthropogenic soils, which are known as a model of organic matter. Knowledge of the chemical structure of HLA is essential for predicting their behavior and benefits in soil.

Because natural HA form complexes with metals (Stevenson, 1994), the study of interaction between metallic ions and HLA is of significant value for predicting whether HLA can assist in the complexation reactions if applied to the soil, and thus the metal bioavailability. A variety of agents has been used for soil washing including

biosurfactants as well as synthetic agents such as ethylenediaminetetraacetic acid (EDTA) (Mulligan et al., 2001, Mulligan, 2009). Despite the efficiency of these agents in removing metals from soils, they cause environmental problems and are high in cost, which justifies the need for more studies to develop new washing agents. In previous research, a solution of HLA from manure compost biochar showed the remediation of soils contaminated by multiple metals (Kulikowska et al., 2015); the same was shown for HLA from composted sewage sludge (Piccolo et al., 2019). In addition, the potential of HLA extracted from hydrochars produced with crude waste biomass was presented (Yang et al., 2019a). In that case, HLA from hydrochars produced with by-products of the sugarcane industry were shown to act in complexation reactions between metals and active sites on the HLA surface.

The fluorescence excitation emission matrix (EEM) has gained prominence in the characterization of organic matter and its interaction with metallic species (Elkins and Nelson, 2002). The analytical potential of fluorescence EEM spectra coupled with chemometric tools such as Parallel Factor Analysis (PARAFAC) has been successfully realized for this type of analysis (Mounier et al., 2011; Nouhi et al., 2018; Stedmon and Bro, 2008; Tadini et al., 2019; Yuan et al., 2015). Moreover, PARAFAC has also been used in the characterization of dissolved organic matter (DOM) of biochars produced with different biomass content (El-Naggar et al., 2020; Rajapaksha et al., 2019; Yang et al., 2019b). Further, because different chemical species have different fluorescence lifetimes, it is also possible to study organic matter–metal interaction through time-resolved fluorescence (TRF), particularly in complex samples such as HA and HLA (Nouhi et al., 2018).

Thus, the chemical characterization of HLA from hydrochars obtained with sugarcane industry by-products was conducted, and the results were compared with that

of HA from TM. In addition, the interaction of HA and HLA with Cu(II) ions by fluorescence quenching was studied to provide quantitative data on the complexation capacity (CC), concentration of binding sites (CL), and conditional stability constant (K). TRF as a complementary technique of fluorescence quenching was used to investigate the interaction by measuring the fluorescence lifetime and its variation with the addition of metal. Thus, the present study can provide a new perspective for analyzing Cu(II)–HLA interactions and the potential of HLA as a complexing agent in the remediation of soils polluted by metals.

2. Materials and methods

2.1 *Terra Mulata* sampling

Soil sampling was performed following the 2000 United States Environmental Protection Agency (EPA) method (US EPA, 2000). For this study, three different areas of TM were selected. The first TM soil was obtained from an open area region containing native vegetation and low vegetation cover (TM I; 3°04′05.45″ S and 58°33′51.11″ W); the second was taken from a closed area region containing native vegetation (TM II; 3°04′05.17″ S and 58°34′11.68″ W); and the third was collected near cultivated areas (TM III; 3°03′59.15″ S and 58°27′04.64″ W). All areas are located near Itacoatiara city in the Amazonas State (Brazil). (SISBio collection was authorized by the Chico Mendes Institute for Biodiversity Conservation, n ° 50042 -2, and registered in the National System for the Management of Genetic Heritage and Associated Traditional Knowledge (SisGen), No. A0018C2.) Soil samples were collected from the 0 to 30 cm deep layer, air-dried, and subsequently sieved through a 2 mm mesh for removal of plant debris and fragments.

2.2 Hydrothermal carbonization and recarbonization process

HTC was performed using vinasse and sugarcane bagasse, in which the vinasse was used to produce the hydrothermal medium (Melo et al., 2017; Silva et al., 2017). The HTC processes were conducted in a Teflon® closed reactor coated with stainless steel. Each mixture (Table 1) was heated in a muffle furnace at 230 °C for 13 h. Then, the reactor was cooled in an ice bath, and the suspension was filtered under vacuum filtration to separate the hydrochar from the process water. The hydrochar was washed with distilled water until constant pH was reached and was then dried at 50 °C until constant mass was achieved. The process water generated in the HTC process was used in the recarbonization process to produce the hydrothermal medium for sugarcane bagasse carbonization. The subsequent steps after carbonization, i.e., filtration, hydrochar washing, and drying, were the same.

Table 1

2.3 Extraction of humic acids and humic-like acids

The extractions were performed following the recommendations of the International Humic Substances Society (IHSS) (Swift, 1996). HS were extracted from TM at a proportion of 1:10 (soil:extractor). Thus, the extraction was conducted in 100 g of soil to 1 L of solution (NaOH 0.1 mol L^{-1}) under nitrogen flow for 4 h. The solution extracted was acidified with HCl (6 mol L^{-1}) to reach pH~1. Thus, HA were precipitated, and fulvic acids remained in the supernatant. Subsequently, the HA were separated by centrifugation, dialyzed using a Fisherbrand apparatus with a molecular weight cut-off at 6,000–8,000 Da, and freeze-dried.

The method was modified for the extraction of humic-like substances (Jindo et al., 2016). Those from hydrochars were extracted at a proportion of 1:10 (hydrochar:extractor) using NaOH (0.1 mol L^{-1}) under nitrogen flow for 4 h. This

151 procedure was repeated, with the same hydrochar portion until the final extract
152 (supernatant phase) showed a lighter color. HLA were obtained by the pH difference,
153 with HCl (6 mol L^{-1}) to pH~1, and was separated from the fulvic-like acids by
154 centrifugation. Finally, the extracts of HLA obtained from each extraction step were
155 combined, dialyzed, and freeze-dried.
156
157 **2.4 Characterization of humic acids and humic-like acids**
158 **2.4.1 Elemental analysis**
159 Elemental analyses were performed on solids using an elemental analyzer (2400
160 Series II CHNS/O, Perkin Elmer, Walther, Massachusetts, USA). The oxygen content
161 was determined according to the difference, i.e., O% = 100 - (C, H, N, S + ashes). The
162 ash content was determined in a muffle furnace at 750 °C for 4 h. The C, H, N, S, and O
163 contents were recalculated on an ash-free basis. The H/C, O/C, and C/N atomic ratios
164 were determined by elemental analysis (Giovanela et al., 2010; Stevenson, 1994).
165
166 **2.4.2 Infrared spectroscopy**
167 Infrared spectra were obtained using an attenuated total reflectance (ATR)-
168 coupled spectrophotometer (FTIR; Spectrum Two UATR, Perkin Elmer, Walther,
169 Massachusetts, USA). The solid material was placed directly on the ATR crystal and
170 was analyzed at a spectral range of 4000–400 cm^{-1} with 20 scans and a resolution of 4
171 cm^{-1}.
172
173 **2.4.3 Ultraviolet–visible spectroscopy**
174 The ultraviolet-visible (UV–Vis) scanning spectra were obtained by employing a
175 UV–Vis spectrophotometer (UV-2600, Shimadzu, Japan) at a range of 200–700 nm. HA

and HLA solutions (10 mg L^{-1}) in total organic carbon (TOC; TOC-VCSN Shimadzu, Japan) were diluted in 0.05 mol L^{-1} of $NaHCO_3$ at pH 8. From the spectra, the ratios E_{465}/E_{665} (E4/E6) and E_{270}/E_{407} (E2/E4) were calculated. These ratios have been used to describe the degree of aromatic ring condensation and the presence of lignin derivatives, respectively (Budziak et al., 2004; Canellas and Façanha, 2004).

2.4.4 Solid-state ^{13}C–CPMAS–NMR spectroscopy

Solid-state ^{13}C–cross-polarized magic angle spinning (CPMAS)–nuclear magnetic resonance (NMR) characterization was performed by employing a Bruker AVANCE 400 MHz spectrometer (Bruker, Billerica, Massachusetts, USA) equipped with a magic angle spin (MAS) probe. A zircon cylindrical rotor with a diameter of 4.0 mm was packed with 80 mg of sample. The spectra were acquired by using a rotor rotation frequency of 10 kHz, recycle time of 1 s, and 5,000 scans. The spectral areas were integrated and divided into seven chemical shifts: C-alkyl (0–45 ppm), C-methoxyl (45–60 ppm), O-alkyl-C (60–110 ppm), aryl-C (110–145 ppm), phenol-C (145–160 ppm), carboxyl-C (160–190 ppm), and carbonyl-C (190–220 ppm). According to the area integration, the aromaticity (ARM), alkyl (A/AO), and hydrophobicity (HB/HI) indices were calculated. (Monda et al., 2018).

2.5 Interaction of humic acids and humic-like acids with Cu(II)

2.5.1 Fluorescence quenching

Studies involving interaction with Cu(II) ions were performed using 10 mg L^{-1} of HA or HLA in a buffer medium with 0.1 mol L^{-1} 4-(2-hydroxyethyl)-1-piperazineethanesulfonic acid (HEPES) at pH 7.0. Titration experiments were performed in 13 cuvettes for each HA or HLA sample with various concentrations of

Cu(II) ($Cu(ClO_4)_2 \cdot 6H_2O$), ranging from 0 mg L^{-1} to 11.2 mg L^{-1}. The equilibrium time of 30 min was determined on the basis of changes observed in the fluorescence signal. Fluorescence measurements were performed using a spectrofluorometer (F4500, Hitachi, Santa Clara, California, USA) equipped with a 450 W xenon lamp. The spectra were acquired in the scan ranges of 220–700 nm for emission and 220–500 nm for excitation, with both slits fixed at 5 nm. The scan speed was set at 2,400 nm min^{-1}, and the detector voltage was 700 V. The obtained EEM spectra were treated by using the PARAFAC chemometric model. The number of components responsible for fluorescence was defined by using the core consistency diagnostic (CORCONDIA) (Mounier et al., 2011). The density of binding sites (CL) as well as the conditional stability constant (K) were determined following the metal complexation model proposed by Ryan and Weber (1982), as represented by

$$M + L \leftrightarrow ML, \quad (1)$$

where *L* is a free complexing site, *M* is the free or uncomplexed metal, and *ML* is the complex. Based on this reaction, the conditional stability constant can be calculated as

$$K = [ML] / [M][L]. \quad (2)$$

Metal and complexing sites follow a mass balance in solution:

$$CL = [ML] + [L], \quad (3)$$

$$CM = [ML] + [M], \quad (4)$$

where *CL* and *CM* represent the total concentration of complexing sites and the metal in the solution system, respectively.

2.5.2 Time-resolved fluorescence

Three samples were selected from the data obtained from the fluorescence quenching experiment, i.e., three total copper concentrations for each HA and HLA

interaction. The first contained no concentration of copper (C_0), whereas $C_{0.7}$ and $C_{5.6}$ contained 0.7 mg L^{-1} and 5.6 mg L^{-1}, respectively. Prior to each measurement, the prepared solution was bubbled with nitrogen for 10 min to prevent photodegradation. TRF experiments were performed at 266 nm from the fourth harmonic generation from a nanosecond laser Nd:YAG (Quanta-Ray INDI, Spectra Physic, Germany), and excitation (1024 nm) occurred with a pulse width of 5 ns and a repetition of 20 Hz. Six hundred spectra were accumulated at each time step of 0.2 ns with an optical fiber and were detected by an intensified charge-coupled device (CCD) camera with a 35 ns gate width. Data obtained by TRFS were corrected by energy fluctuation and were treated by using a homemade MATLAB® program to obtain the spectral deconvolution and the associated lifetime values.

3. Results and discussion

3.1 Characterization of humic acids and humic-like acids

Determining the molecular formula of HA and HLA is still a challenge; however, elemental analysis can provide a general idea about their compositions. The elemental analysis and UV–Vis ratios of soil HA and hydrochar HLA samples are shown in Table 2. In general, HA and HLA showed carbon as the main constituent, at 36.6% to 62.2%, followed by oxygen, hydrogen, nitrogen, and sulfur. In addition, HLA RHH_2SO_4 had the highest sulfur content of the samples. Regarding the carbon percentage, the HLA samples showed higher values than did HA.

The O/C, H/C, and C/N atomic ratios (Table 2) based on elemental analysis, have been used to describe the content of oxygenated groups in the molecules, the degree of aromatic ring condensation, and the nitrogen content, respectively (Giovanela et al., 2010; Stevenson, 1994). In general, HA showed higher O/C ratios than those of

HLA, suggesting a greater abundance of oxygen-containing functional groups (Fukushima et al., 2014). The H/C ratio showed that HA, except for the TM II HA, have higher condensation of aromatic rings than do HLA; lower C/N atomic ratios for HA suggest more nitrogen-containing structures (F. Yang et al., 2019).

The UV–Vis spectra of HA have been previously described in the literature and provide little structural information. Generally, however, the overall absorbance decreases with increasing wavelength (Uyguner and Bekbolet, 2005). In this study, both HA and HLA showed this behavior; the spectra are shown in the supplementary material (Figure S1). For better interpretation of UV–Vis analysis, the absorbance ratios at certain wavelengths were utilized. The E_{465}/E_{665} absorbance ratio is related to the degree of condensation of aromatic rings. Values lower than 4 indicate compounds with more condensed aromatic groups (Canellas and Façanha, 2004; Stevenson, 1994; He et al., 2016). The E_{270}/E_{407} absorbance ratio refers to the presence of lignin derivatives, of which the content is directly proportional to this value (Budziak et al., 2004). This ratio might be indicative for organic matter studies because lignin is involved in the formation of both soils and hydrochars. The obtained parameters are presented in Table 2.

HA showed a higher degree of aromatic condensation than HLA. Furthermore, the lower number of compounds with lignin structures might be linked to greater decomposition of organic matter.

Table 2

The FTIR spectra (Figure 1a and 1b) showed that both HA and HLA have typical features of HS (Esteves et al., 2009; Fernandes et al., 2010; Giovanela et al., 2010). In the 3500–3300 cm^{-1} region, larger bands were observed for HA. However, the bands for HLA were more defined and might be related to N-H stretching of amines or

amides and O-H stretching of alcohols and phenols (Dick et al., 2003). The same result was observed for the C-H stretching of aliphatic methyl and methylene groups near 2900 cm^{-1}. In the 1730–1710 cm^{-1} region, low intensity of C=O stretching of carboxylic acids or ketones was found for HA (Figure 1a), and a slight shoulder was observed for the HLA samples (Figure 1b) (Senesi et al., 2003). Bands in the 1620–1600 cm^{-1} regions were associated with aromatic C=C stretching (Stevenson, 1994). C-H bending of CH_3 and deformation of CH_2 and CH_3 structures were observed in the 1420–1380 cm^{-1} region for HLA but not for HA. All spectra showed C-O-C stretching at approximately 1250–1030 cm^{-1}, likely resulting from polysaccharides; stretching in esters, alcohols, and phenols was also observed. In addition, Si-O stretching bands were identified in the 825–750 cm^{-1} region (Giovanela et al., 2010; Stevenson, 1994).

Figure 1

The ^{13}C–CPMAS–NMR spectra of HA and HLA are shown in Figure 2. Both samples showed complex chemical compositions, with peaks related to aromatic and aliphatic carbons, substituted or not by heteroatoms, and different intensities. The following peaks were observed in all samples: 0–45 ppm, attributed to the presence of alkyl carbons of methyl and methylene groups; 45–60 ppm for carbons linked to methoxyl groups and nitrogen compounds (C-N); 60–110 ppm, indicating the presence of oxygen-substituted carbons and alkyl groups (O-alkyl); 110–145 ppm, attributed to the presence of aromatic groups; and 145–160 ppm for substituted aromatic carbons, 160–190 ppm for carbonyl groups, and 190–220 ppm for carboxylic groups in the structures of HA and HLA (Mazzei and Piccolo, 2012; Monda et al., 2017; Spaccini and Piccolo, 2009; Tadini et al., 2015).

Chemical shifts near 15 ppm were assigned to short-chain aliphatic structures, whereas those at 30 ppm were assigned to long-chain aliphatic structures attributed to

lipid compounds, such as plant waxes and biopolyesters (Francioso et al., 2002; Monda et al., 2017; Spaccini et al., 2019). These peaks were more intense in the HLA samples (Figure 2). The peak at 54 ppm, related to the presence of methoxyl carbons in both guaiacil and syringyl units of lignin fragments, as well as Cα of oligo- and polypeptides (Monda et al., 2017), was present for both HA and HLA except in those in which sulfuric acid was used as an additive (Figure 2).

The peaks in the 71–74 ppm range were more evident in HA and are typical of O-akyl-C in mono and polysaccharides, in which the centered peak at 72 ppm is attributed to the overlapping of carbon numbers 2, 3, and 5 in the pyranosidic cellulose and hemicellulose structures, referred to as C-2, C-3, and C-5, respectively (Monda et al., 2017; Spaccini and Piccolo, 2009). Unsubstituted aromatic carbons were responsible for the intense signal at 130 ppm (Monda et al., 2017) in the HA and HLA structures, whereas their analogs containing -OH, -OCH_3, and -NH_2 groups were found in the 145–160 ppm region. The signal at 174 ppm corresponds to carboxylic acids, and the low signal at 190–220 ppm refers to carbonyl groups of ketones, amides, and aldehyde (Mao et al., 2011) in the HA and HLA, as shown in Figure 2.

Figure 2

By employing spectral integration, it is possible to estimate the distribution of carbons in the HA and HLA structures as well as some indices such as A/AO, ARM, and HB/HI, as shown in Table 3. These indices are related to the biochemical stability of different organic compounds. The HA showed aromatic compounds as the main constituents, whereas HLA showed the presence of aromatic and aliphatic carbons (Table 3). The ARM index was similar for both materials. Higher HB/HI index values indicate the incorporation of hydrophobic moieties in HLA (Bento et al., 2019). Furthermore, the natural HA were more hydrophilic than those HLA obtained from

HTC, which is indicated by the decrease in the A/OA index (Table 3). All of these factors, such as presence or absence, greater incorporation of functional groups or not in humic and humic-like acids, influence the binding properties with metal ions.

Table 3

3.2 Interaction of humic acids and humic-like acids with Cu(II)

3.2.1 Fluorescence quenching

The interactions of HA and HLA with Cu(II) ions were evaluated by fluorescence quenching; the concentration of each humic extract was 10 mg L^{-1}. Other authors have used this concentration value of humic extract in experiments for the same purpose: to avoid inner filters (Guo et al., 2015; Yuan et al., 2015). The quenching results were combined with the PARAFAC multivariate statistical tool, in which the complex signal of the fluorescence spectra was decomposed into simple and independent components.

Thus, a three-component model was found for HA quenching experiments with a good CORCONDIA value (94.75%). The components are shown in Figure 3. Component 1 (Figure 3a) had a main peak at [λ_{Ex} 300 nm/λ_{Em} 475 nm], which is typical of humic-like substances. Component 2 (Figure 3b) had a secondary peak at [λ_{Ex} 275 nm/λ_{Em} 530 nm], which is associated with low-energy peaks known to be typically linked to terrestrial HA (Matthews et al., 1996; Stedmon et al., 2003), and a main peak at [λ_{Ex} 475 nm/λ_{Em} 530 nm], which is typical of lignin-derived terrestrial HA. In addition, component 1 showed a blue shift for fluorescence emission intensity, whereas component 2 demonstrated a red shift, characterizing the presence of simple and complex structures, respectively (Senesi et al., 2003). Conversely, component 3 (Figure 3c) showed no variation in its contribution during the quenching experiments, which is

likely related to a noise factor. Therefore, this component was not considered in the discussion.

A three-component model was also found for the interaction with HLA, with a CORCONDIA value of 97.46%; these components are also shown in Figure 3. Component 1 (Figure 3d) showed a main and a secondary peak at [λ_{Ex} 260 nm/λ_{Em} 425 nm] and [λ_{Ex} 340 nm/λ_{Em} 425 nm], respectively. Both components are characteristic of humic substances from terrestrial environments (Coble, 1996; Matthews et al., 1996; Stedmon et al., 2003). Component 2 (Figure 3e) had a main peak at [λ_{Ex} 275 nm/λ_{Em} 510 nm] and a secondary peak at [λ_{Ex} 400 nm/λ_{Em} 510 nm]. The main peak was classified as typically humic-like, and the secondary peak refers to soil fulvic acid. Component 3 (Figure 3f) showed no fluorescence variation; therefore, similar to that for HA, it was not considered in the discussion.

Figure 3

It is possible to obtain the fluorescence contribution of each component in the sample, known as the score, depending on the metal addition. The initial humic extracts were considered as 100%, and the contribution decreased with the addition of metal. Figure 4a shows the scores of components 1 and 2 regarding the interaction of TM I HA with Cu(II) ions, and Figure 4b shows those regarding the interaction of HH_2SO_4 HLA. All three HA samples showed similar behavior; additional graphs are given in the supplementary material (Figure S2). The four HLA samples also showed similarly behavior, as shown in the supplementary material (Figure S3).

Figure 4

The fluorescence quenching curve for the first component of HA and Cu(II) (Figure 4a) showed a fluorescence intensity decay of approximately 85.6%, and the second component had a value of 92.5%. This significant decay in fluorescence

contribution is attributed to the formation of a complex in which the fluorescence quantum yield changed (Mounier et al., 2011; Tadini et al., 2019). Moreover, the interaction with Cu(II) was shown to influence the optical properties of organic matter. For the interaction between HLA and Cu(II) (Figure 4b), the fluorescence intensity decay for the first component remained at approximately 67.3%, whereas that for the second was approximately 58.2%. The decrease in fluorescence intensity of the HA components appeared at the first concentrations of Cu(II). For the HLA components, an increase in copper concentration was necessary for better visualization of the quenching phenomenon.

Optimization of the data using the 1:1 (ligand:metal) complexation model proposed by Ryan and Weber (1982) enables evaluation of the equilibrium parameters, particularly CL and K, of which CL is the concentration of binding sites capable of forming a complex and K is the conditional stability constant of the complex formed.

The equilibrium parameters for the HA and HLA experiments, including CL, log K, CC, and the bias values, are given in Table 4. To evaluate the 1:1 complexation model, bias was used as an optimization parameter. Bias is the sum of the absolute value of the difference between the experimental and calculated fluorescence logarithm intensity. In this study, the bias values ranged from 0.27 to 4.18, which are lower than those found in the literature (Tadini et al., 2019). Therefore, the experimental data fit well in the theoretical model (Table 4). The titration curves of the theoretical and experimental values for components 1 and 2 of HA and components 1 and 2 of HLA with Cu(II) can be found in the supplementary material (Figures S4 and S5).

Table 4

For HA components 1 and 2, the log K values remained in the ranges of 5.30–5.41 and 5.58–5.60, respectively; for HLA components 1 and 2, these values were in the

ranges of 4.88–4.90 and 5.06–5.09, respectively. The HA components showed higher values for log K and both blue and red shifts in the fluorescence emission wavelengths. In addition, the fluorophores exhibited different chemical structures and compounds with good binding capacities, which is confirmed by Figure 3a, b. The HLA components showed similar values for log K compared with HA and values either similar to or higher than those found in the literature for other types of HA (Fuentes et al., 2013; Plaza et al., 2005; Tadini et al., 2019). Blue and red shifts were also observed (Figure 3d, e); therefore, the fluorophores have different chemical structures and are weakly bonded compared to HA.

It is noteworthy that TM, which occurs in the Amazon, is different from common soils and has high fertility because of the carbon stock and long-term nutrients. This fact was demonstrated by good interaction with the metal ion (log K 5.30–5.60). HLA showed higher log K values than those found in Spodosols, which also occur in the Amazon region (log K 3.79–5.32) (Tadini et al., 2019), or peat and leonardite (log K 4.58–5.10) (Fuentes et al., 2013). This indicates that the organic matter extracted from hydrochars can also interact satisfactorily with Cu(II) ions to form complexes. Additionally, by using the CL values, it was also possible to determine the CC for all components 1 and 2 from HA and HLA. This parameter was obtained by dividing the CL values by the carbon content. CC represents the concentration of binding sites per gram of carbon available to interact with Cu(II) ions. Table 4 also shows the CC values for HA and HLA components 1 and 2.

Both HLA components 1 and 2 showed higher concentrations of binding sites per gram of carbon for interaction with Cu(II) ions than those of HA; and the highest value was observed for RHH_2SO_4 HLA. Regarding log K, the CC values were also higher than those found in the literature for HA from soils, peat, or leonardite (Fuentes

et al., 2013; Plaza et al., 2005; Tadini et al., 2019). Tadini et al. (2019) determined the CC of components by fluorescence quenching for HA extracted from Amazonian Spodosols with Cu(II) ions and found CC values ranging from 0.01–0.13 mmol of Cu g^{-1} C. The values found in this study for HA extracted from TM were higher, indicating both a larger amount of complexing sites and an affinity of organic matter with the metallic ion. The same result was observed for HLA, indicating that if applied to the soil, it could help in the complexation reactions.

Previous research indicates that the high stability constants of HA are associated with increased oxygen-containing groups such as -COOH and -OH as well as π-π bonds in the C=C of aromatic rings (Guo et al., 2012, 2015). These functional groups were observed for HA and HLA by using both FTIR and ^{13}C NMR techniques. The results show that the predominance of conjugate and aromatic structures as well as oxygen-containing groups are responsible for HA complexation, and for HLA, both aromatic and aliphatic groups are responsible. Pearson established the concept of chemical bonding regarding the affinity of different metals to different ligands (Pearson, 1963). It was reported that chemical species can be classified as “hard” and “soft” or “borderline” acids and bases and that the concepts of “hardness” and “softness” can help to interpret the mechanism of complexation. Soft acids tend to have preferential interaction by soft bases, whereas hard acids tend to bind with hard bases; borderline acids form considerably stable bonds with both hard and soft bases, although it is sometimes difficult to determine the preferential order for bond formation. These concepts partly explain the stability of chemical compounds (Pearson, 1963).

As observed in the ^{13}C NMR spectra and in the H/C, O/C, and C/N atomic ratios, HA and HLA showed similar ARM, although HA showed a higher percentage of oxygenated groups and nitrogen in its structure. The Cu(II) ion used in this study is a

451 borderline acid and interacts with both hard bases such as oxygen and soft bases such as
452 nitrogen; thus, HA had a stronger interaction with Cu(II) because of their molecular
453 structures. Lu and Allen (2002) found that the interaction of DOM with Cu(II) ions is
454 attributed mostly to phenol OH groups, and Hernández (2006) showed a positive and
455 significant correlation with carboxylic acid and phenols. Moreover, the presence of
456 large amounts of functional groups and π-π bonds of aromatic rings should confer a
457 greater complexation capacity for HA from TM; however, this did not occur potentially
458 owing to the different molecular arrangements. Further, it is possible that the functional
459 groups and aromatic carbons in HA structures were already occupied by another metal
460 or more condensed aromatic rings. All of these factors can affect the behavior of Cu(II)
461 ions in both soils and hydrochar extracts. Conversely, HLA showed more binding sites
462 available for interaction considering the amount of carbon in the sample, and thus
463 greater complexation capacity.
464
465 **3.2.2 Time-resolved fluorescence**
466 In addition, fluorescence quenching can be induced by two mechanisms. The first
467 is dynamic quenching, which is caused by collision with a quencher and occurs during
468 the lifetime of the excited state, affecting the fluorescence lifetime. The second is static
469 quenching, which occurs when a ground-state non-fluorescent complex is formed, and
470 the lifetimes of the fluorescent ligand and complex are unaffected (Lakowics, 1999).
471 Therefore, TRF is the best method for distinguishing whether static or dynamic
472 quenching occurs during the interaction of organic matter with copper.
473 Figure 5a and 5b show the fluorescence average lifetime distribution of HA and
474 HLA complexes with copper, respectively. The deconvolution of TRF results in the HA
475 complexes show that the decay was mono-exponential (τ_1) decay containing only one

lifetime. The average lifetime values observed were shorter, at approximately 5–6 ns, which is associated with the simple structure of HA. This average lifetime can be attributed to component 1 (Figure 3a) observed in PARAFAC. The average lifetime of component 2, with emission at 530 nm (Figure 3b) did not appear in the results because the emission spectra in TRF reached only 510 nm owing to laser leakage at 532 nm.

The best fit for HLA complexes showed a bi-exponential decay (τ_1 and τ_2), the average lifetimes of which were approximately 4 ns and 14 ns, respectively. These results fit well with the PARAFAC for HLA, which showed two components, one with a simple structure (component 1) and the other with a complex structure (component 2), reflecting lower and higher lifetimes, respectively. The first average lifetime τ_1 was almost the same as that for HA (Figure 3d). Lifetime τ_2 can be associated with component 2 (Figure 3e), which has a more complex fluorophore structure.

Figure 5

The average lifetime values were determined to be independent of the copper concentration for HA and HLA interaction (Figure 5). This suggests that the mechanism of Cu(II) quenching by fluorescence occurs with a non-fluorescent ground-state complex, i.e., the complexation occurs by static quenching. Nouhi (2018) also reported static quenching and similar lifetime values for interaction between Cu(II) and Eu(III) with HA extracted from the Saint Lawrence Estuary in Canada (Nouhi, 2018).

In summary, this study demonstrated the potential of fluorescence quenching and TRF for evaluating the interaction between metallic species and organic matter, which provides insight into the interaction mechanism. No previous studies related to fluorescence quenching and lifetime measurements of HA extracted from Amazonian TM and HLA from hydrochars with metallic species are available for comparison with the results achieved here.

4. Conclusion

HLA were obtained by NaOH aqueous solution extraction from hydrochar produced by the HTC process using sugarcane industry by-products. These HLA showed greater complexation capacity with Cu(II) ions than the HA extracted from TM. In addition, similar values for stability constants for both HA and HLA were observed. The interaction with Cu(II) in HLA occurs by both aromatic and aliphatic moieties, showing that π-π interaction and oxygen groups are not the only factors that play important roles in the CC. Furthermore, the TRF for the interaction of metallic species and organic matter showed that the main interaction mechanism was static quenching. These results show that HLA extracted from hydrochars can be an efficient approach for interacting with metals and can be a new tool for remediating areas contaminated by metals.

Acknowledgments

This work was supported by the São Paulo Research Foundation (FAPESP) (grants 15/22954-1, 17/26718-6, and 18/15733-7). J.V.S acknowledges a scholarship from FAPESP (grants 17/05408-9 and 18/09914-9). O.P.F acknowledges financial support from FUNCAP (PRONEX PR2-0101-00006.01.00/15). The authors thank Dr. Maurício Boscolo for offering assistance with the FTIR analysis (process 2017/13230-5) and Dr. Isabella Constatino and Dr. Fabiana Paschoal for their assistance with soil sampling.

References

Andreazza, R., Okeke, B.C., Lambais, M.R., Bortolon, L., de Melo, G.W.B., de Oliveira

526 Camargo, F.A., 2010. Bacterial stimulation of copper phytoaccumulation by
527 bioaugmentation with rhizosphere bacteria. Chemosphere 81, 1149–1154.
528 https://doi.org/10.1016/j.chemosphere.2010.09.047

529 Bento, L. R.; Melo, C. A.; Ferreira, O. P.; Moreira, A. B.; Mounier, S.; Piccolo, A.;
530 Spaccini, R.; Bisinoti, M.C., 2020. Humic extracts of hydrochar and Amazonian
531 Dark Earth: Molecular characteristics and effects on maize seed germination. Sci.
532 Total Environ. https://doi.org/10.1016/j.scitotenv.2019.135000

533 Bento, L.R., Melo, C.A., Ferreira, O.P., Moreira, B., Mounier, S., Piccolo, A., Spaccini,
534 R., Bisinoti, M.C., 2019. Humic extracts of hydrochar and Amazonian Dark Earth:
535 Molecular characteristics and effects on maize seed germination. Sci. Total
536 Environ. 135000. https://doi.org/10.1016/j.scitotenv.2019.135000

537 Budziak, C.R., Maia, C.M.B.F., Mangrich, A.S., 2004. Transformações químicas da
538 matéria orgânica durante a compostagem de resíduos da indústria madeireira.
539 Quim. Nova 27, 399–403. https://doi.org/10.1590/S0100-40422004000300007

540 Canellas, L.P., Façanha, A.R., 2004. Chemical nature of soil humified fractions and
541 their bioactivity. Pesqui. Agropecu. Bras. 39, 233–240.
542 https://doi.org/10.1590/S0100-204X2004000300005

543 Chen, J., Chen, H., Zhang, X.W., Lei, K., Kenny, J.E., 2015. Combination of a Copper-
544 Ion Selective Electrode and Fluorometric Titration for the Determination of
545 Copper(II) Ion Conditional Stability Constants of Humic Substances. Acta radiol.
546 56, 1293–1302. https://doi.org/10.1366/14-07835

547 Coble, P.G., 1996. Characterization of marine and terrestrial DOM in the seawater using
548 exciting-emission matrix. Mar. Chem. 51, 325–346. https://doi.org/10.1016/0304-
549 4203(95)00062-3

Dick, D. P.; Santos, J. H. Z.; Ferranti, E.M., 2003. Chemical Characterization and Infrared Spectroscopy of Soil Organic Matter From Two Southern Brazilian Soils (1). Rev. Bras. Cienc. do Solo 27, 29–39. https://doi.org/10.1590/S0100-06832003000100004

El-Naggar, A., Lee, M.H., Hur, J., Lee, Y.H., Igalavithana, A.D., Shaheen, S.M., Ryu, C., Rinklebe, J., Tsang, D.C.W., Ok, Y.S., 2020. Biochar-induced metal immobilization and soil biogeochemical process: An integrated mechanistic approach. Sci. Total Environ. 698, 134112. https://doi.org/10.1016/j.scitotenv.2019.134112

Elkins, K.M., Nelson, D.J., 2002. Spectroscopic approaches to the study of the interaction of aluminum with humic substances. Coord. Chem. Rev. 228, 205–225. https://doi.org/10.1016/S0010-8545(02)00040-1

Esteves, V.I., Otero, M., Duarte, A.C., 2009. Comparative characterization of humic substances from the open ocean, estuarine water and fresh water. Org. Geochem. 40, 942–950. https://doi.org/10.1016/j.orggeochem.2009.06.006

Fernandes, A.N., Giovanela, M., Esteves, V.I., Sierra, M.M. de S., 2010. Elemental and spectral properties of peat and soil samples and their respective humic substances. J. Mol. Struct. 971, 33–38. https://doi.org/10.1016/j.molstruc.2010.02.069

Francioso, O., Sánchez-Cortés, S., Casarini, D., Garcia-Ramos, J. V., Ciavatta, C., Gessa, C., 2002. Spectroscopic study of humic acids fractionated by means of tangential ultrafiltration. J. Mol. Struct. 609, 137–147. https://doi.org/10.1016/S0022-2860(01)00971-1

Fregolente, L.G., Miguel, T.B.A.R., de Castro Miguel, E., de Almeida Melo, C., Moreira, A.B., Ferreira, O.P., Bisinoti, M.C., 2018. Toxicity evaluation of process

574 water from hydrothermal carbonization of sugarcane industry by-products.
575 Environ. Sci. Pollut. Res. 1–11. https://doi.org/10.1007/s11356-018-1771-2

576 Fu, F., Wang, Q., 2011. Removal of heavy metal ions from wastewaters: A review. J.
577 Environ. Manage. 92, 407–418. https://doi.org/10.1016/j.jenvman.2010.11.011

578 Fuentes, M., Olaetxea, M., Baigorri, R., Zamarreño, A.M., Etienne, P., Laîné, P., Ourry,
579 A., Yvin, J.C., Garcia-Mina, J.M., 2013. Main binding sites involved in Fe(III) and
580 Cu(II) complexation in humic-based structures. J. Geochemical Explor. 129, 14–
581 17. https://doi.org/10.1016/j.gexplo.2012.12.015

582 Fukushima, M., Okabe, R., Nishimoto, R., Fukuchi, S., Sato, T., Terashima, M., 2014.
583 Adsorption of pentachlorophenol to a humin-like substance-bentonite complex
584 prepared by polycondensation reactions of humic precursors. Appl. Clay Sci. 87,
585 136–141. https://doi.org/10.1016/j.clay.2013.10.022

586 Giovanela, M., Crespo, J.S., Antunes, M., Adamatti, D.S., Fernandes, A.N., Barison, A.,
587 Da Silva, C.W.P., Guégan, R., Motelica-Heino, M., Sierra, M.M.D., 2010.
588 Chemical and spectroscopic characterization of humic acids extracted from the
589 bottom sediments of a Brazilian subtropical microbasin. J. Mol. Struct. 981, 111–
590 119. https://doi.org/10.1016/j.molstruc.2010.07.038

591 Glaser, B., Balashov, E., Haumaier, L., Guggenberger, G., Zech, W., 2000. Black
592 carbon in density fractions of anthropogenic soils of the Brazilian Amazon region.
593 Org. Geochem. 31. https://doi.org/10.1016/S0146-6380(00)00044-9

594 Guo, X., Jiang, J., Xi, B., He, X., Zhang, H., Deng, Y., 2012. Study on the spectral and
595 Cu (II) binding characteristics of DOM leached from soils and lake sediments in
596 the Hetao region. Environ. Sci. Pollut. Res. 19, 2079–2087.
597 https://doi.org/10.1007/s11356-011-0704-0

598 Guo, X. jing, Zhu, N. min, Chen, L., Yuan, D. hai, He, L. sheng, 2015. Characterizing
599 the fluorescent properties and copper complexation of dissolved organic matter in
600 saline-alkali soils using fluorescence excitation-emission matrix and parallel factor
601 analysis. J. Soils Sediments 15, 1473–1482. https://doi.org/10.1007/s11368-015-
602 1113-7

603 He, E., Lü, C., He, J., Zhao, B., Wang, J., Zhang, R., Ding, T., 2016. Binding
604 characteristics of Cu2+ to natural humic acid fractions sequentially extracted from
605 the lake sediments. Environ. Sci. Pollut. Res. 23, 22667–22677.
606 https://doi.org/10.1007/s11356-016-7487-2

607 Hernández, D., Plaza, C., Senesi, N., Polo, A., 2006. Detection of Copper(II) and
608 zinc(II) binding to humic acids from pig slurry and amended soils by fluorescence
609 spectroscopy. Environ. Pollut. 143, 212–220.
610 https://doi.org/10.1016/j.envpol.2005.11.038

611 Hladun, K.R., Parker, D.R., Trumble, J.T., 2015. Cadmium, Copper, and Lead
612 Accumulation and Bioconcentration in the Vegetative and Reproductive Organs of
613 Raphanus sativus: Implications for Plant Performance and Pollination. J. Chem.
614 Ecol. 41, 386–395. https://doi.org/10.1007/s10886-015-0569-7

615 Jindo, K., Sánchez-Monedero, M.A., Matsumoto, K., Sonoki, T., 2019. The efficiency
616 of a low dose of biochar in enhancing the aromaticity of humic-like substance
617 extracted from poultry manure compost. Agronomy 9, 1–10.
618 https://doi.org/10.3390/agronomy9050248

619 Jindo, K., Sonoki, T., Matsumoto, K., Canellas, L., Roig, A., Sanchez-Monedero, M.A.,
620 2016. Influence of biochar addition on the humic substances of composting
621 manures. Waste Manag. 49, 545–552.

https://doi.org/10.1016/j.wasman.2016.01.007

Kabadayi Catalkopru, A., Kantarli, I.C., Yanik, J., 2017. Effects of spent liquor recirculation in hydrothermal carbonization. Bioresour. Technol. 226, 89–93. https://doi.org/10.1016/j.biortech.2016.12.015

Kulikowska, D., Gusiatin, Z.M., Bułkowska, K., Klik, B., 2015. Feasibility of using humic substances from compost to remove heavy metals (Cd, Cu, Ni, Pb, Zn) from contaminated soil aged for different periods of time. J. Hazard. Mater. 300, 882–891. https://doi.org/10.1016/j.jhazmat.2015.08.022

Lakowics, J.R., 1999. Principles of fluorescence spectroscopy, 2nd ed. New York: Kluwer Academic/ Plenum Publisher.

Lesmana, S.O., Febriana, N., Soetaredjo, F.E., Sunarso, J., Ismadji, S., 2009. Studies on potential applications of biomass for the separation of heavy metals from water and wastewater. Biochem. Eng. J. 44, 19–41. https://doi.org/10.1016/j.bej.2008.12.009

Li, Z., Ma, Z., van der Kuijp, T.J., Yuan, Z., Huang, L., 2014. A review of soil heavy metal pollution from mines in China: Pollution and health risk assessment. Sci. Total Environ. 468–469, 843–853. https://doi.org/10.1016/j.scitotenv.2013.08.090

Lu, Y., Allen, H.E., 2002. Characterization of copper complexation with natural dissolved organic matter (DOM) - Link to acidic moieties of DOM and competition by Ca and Mg. Water Res. 36, 5083–5101. https://doi.org/10.1016/S0043-1354(02)00240-3

MacKie, K.A., Müller, T., Kandeler, E., 2012. Remediation of copper in vineyards - A mini review. Environ. Pollut. 167, 16–26. https://doi.org/10.1016/j.envpol.2012.03.023

Mao, J., Chen, N., Cao, X., 2011. Characterization of humic substances by advanced solid state NMR spectroscopy: Demonstration of a systematic approach. Org. Geochem. 42, 891–902. https://doi.org/10.1016/j.orggeochem.2011.03.023

Matthews, B.J.H., Jones, A.C., Theodorou, N.K., Tudhope, A.W., 1996. Excitation-emission-matrix fluorescence spectroscopy applied to humic acid bands in coral reefs. Mar. Chem. 55, 317–332. https://doi.org/10.1016/S0304-4203(96)00039-4

Mazzei, P., Piccolo, A., 2012. Quantitative evaluation of noncovalent interactions between glyphosate and dissolved humic substances by NMR spectroscopy. Environ. Sci. Technol. 46, 5939–5946. https://doi.org/10.1021/es300265a

Melo, C.A., Junior, F.H.S., Bisinoti, M.C., Moreira, A.B., Ferreira, O.P., 2017. Transforming sugarcane bagasse and vinasse wastes into hydrochar in the presence of phosphoric acid: an evaluation of nutrient contents and structural properties. Waste and Biomass Valorization 1139–1151. https://doi.org/10.1007/s12649-016-9664-4

Monda, H., Cozzolino, V., Vinci, G., Drosos, M., Savy, D., Piccolo, A., 2018. Molecular composition of the Humeome extracted from different green composts and their biostimulation on early growth of maize. Plant Soil 429, 407–424. https://doi.org/10.1007/s11104-018-3642-5

Monda, H., Cozzolino, V., Vinci, G., Spaccini, R., Piccolo, A., 2017. Molecular characteristics of water-extractable organic matter from different composted biomasses and their effects on seed germination and early growth of maize. Sci. Total Environ. 590–591, 40–49. https://doi.org/10.1016/j.scitotenv.2017.03.026

Mounier, S., Zhao, H., Garnier, C., Redon, R., 2011. Copper complexing properties of dissolved organic matter: PARAFAC treatment of fluorescence quenching.

669 Biogeochemistry 106, 107–116. https://doi.org/10.1007/s10533-010-9486-6

670 Mulligan, C.N., 2009. Recent advances in the environmental applications of
671 biosurfactants. Curr. Opin. Colloid Interface Sci. 14, 372–378.
672 https://doi.org/10.1016/j.cocis.2009.06.005

673 Mulligan, C.N., Yong, R.N., Gibbs, B.F., 2001. Heavy metal removal from sediments
674 by biosurfactants. J. Hazard. Mater. 85, 111–125. https://doi.org/10.1016/S0304-
675 3894(01)00224-2

676 Nouhi, A., 2018. Caractérisation Spectrale et Temporelle par Quenching de
677 Fluorescence des Interactions Matière Organique-Eléments Métalliques. Universté
678 de Toulon.

679 Nouhi, A., Hajjoul, H., Redon, R., Gagné, J.P., Mounier, S., 2018. Time-resolved laser
680 fluorescence spectroscopy of organic ligands by europium: Fluorescence
681 quenching and lifetime properties. Spectrochim. Acta - Part A Mol. Biomol.
682 Spectrosc. 193, 219–225. https://doi.org/10.1016/j.saa.2017.12.028

683 Oliveira, N.C., Paschoal, A.R., Paula, R.J., Constantino, I.C., Bisinoti, M.C., Moreira,
684 A.B., Fregolente, L.G., Santana, A.M., Sousa, F.A., Ferreira, O.P., Paula, A.J.,
685 2018. Morphological analysis of soil particles at multiple length-scale reveals
686 nutrient stocks of Amazonian Anthrosols. Geoderma 311, 58–66.
687 https://doi.org/10.1016/j.geoderma.2017.09.034

688 Pearson, R.G., 1963. Hard and Soft Acids and Bases. J. Am. Chem. Soc. 85, 3533–
689 3539. https://doi.org/10.1021/ja00905a001

690 Piccolo, A., Spaccini, R., De Martino, A., Scognamiglio, F., di Meo, V., 2019. Soil
691 washing with solutions of humic substances from manure compost removes heavy

692 metal contaminants as a function of humic molecular composition. Chemosphere
693 225, 150–156. https://doi.org/10.1016/j.chemosphere.2019.03.019

694 Plaza, C., D'Orazio, V., Senesi, N., 2005. Copper(II) complexation of humic acids from
695 the first generation of EUROSOILS by total luminescence spectroscopy.
696 Geoderma 125, 177–186. https://doi.org/10.1016/j.geoderma.2004.07.012

697 Rajapaksha, A.U., Ok, Y.S., El-Naggar, A., Kim, H., Song, F., Kang, S., Tsang, Y.F.,
698 2019. Dissolved organic matter characterization of biochars produced from
699 different feedstock materials. J. Environ. Manage. 233, 393–399.
700 https://doi.org/10.1016/j.jenvman.2018.12.069

701 Ryan, D.K., Weber, J.H., 1982. Fluorescence Quenching Titration for Determination of
702 Complexing Capacities and Stability Constants of Fulvic Acid. Anal. Chem. 54,
703 986–990. https://doi.org/10.1021/ac00243a033

704 Senesi, N., D'Orazio, V., Ricca, G., 2003. Humic acids in the first generation of
705 EUROSOILS. Geoderma 116, 325–344. https://doi.org/10.1016/S0016-
706 7061(03)00107-1

707 Silva, C.C., Melo, C.A., Soares Junior, F.H., Moreira, A.B., Ferreira, O.P., Bisinoti,
708 M.C., 2017. Effect of the reaction medium on the immobilization of nutrients in
709 hydrochars obtained using sugarcane industry residues. Bioresour. Technol. 237,
710 213–221. https://doi.org/10.1016/j.biortech.2017.04.004

711 Spaccini, R., Cozzolino, V., Di Meo, V., Savy, D., Drosos, M., Piccolo, A., 2019.
712 Bioactivity of humic substances and water extracts from compost made by ligno-
713 cellulose wastes from biorefinery. Sci. Total Environ. 646, 792–800.
714 https://doi.org/10.1016/j.scitotenv.2018.07.334

715 Spaccini, R., Piccolo, A., 2009. Molecular characteristics of humic acids extracted from
716 compost at increasing maturity stages. Soil Biol. Biochem. 41, 1164–1172.
717 https://doi.org/10.1016/j.soilbio.2009.02.026

718 Stedmon, C.A., Bro, R., 2008. Characterizing dissolved organic matter fluorescence
719 with parallel factor analysis: a tutorial. Limnol. Oceanogr. 6, 1–8.
720 https://doi.org/10.4319/lom.2008.6.572

721 Stedmon, C.A., Markager, S., Bro, R., 2003. Tracing dissolved organic matter in aquatic
722 environments using a new approach to fluorescence spectroscopy. Mar. Chem. 82,
723 239–254. https://doi.org/10.1016/S0304-4203(03)00072-0

724 Stemann, J., Putschew, A., Ziegler, F., 2013. Hydrothermal carbonization: Process
725 water characterization and effects of water recirculation. Bioresour. Technol. 143,
726 139–146. https://doi.org/10.1016/j.biortech.2013.05.098

727 Stevenson, F.J., 1994. Humus chemistry: Genesis, composition, and reactions. New
728 York John Wiley Sons.

729 Swift, R.S., 1996. Methods of soil analysis. Part 3. Chemical methods. Soil Sci. Soc.
730 Am. 1011–1020.

731 Tadini, A. M.; Mounier, S.; Milori, D.M.B.P., 2019. Modeling the quenching of
732 fluorescence from organic matter in Amazonian soils. Sci. Total Environ. 698,
733 134067. https://doi.org/10.1016/j.scitotenv.2019.134067

734 Tadini, A.M., Constantino, I.C., Nuzzo, A., Spaccini, R., Piccolo, A., Moreira, A.B.,
735 Bisinoti, M.C., 2015. Characterization of typical aquatic humic substances in areas
736 of sugarcane cultivation in Brazil using tetramethylammonium hydroxide
737 thermochemolysis. Sci. Total Environ. 518–519, 201–208.

https://doi.org/10.1016/j.scitotenv.2015.02.103

Tang, W.W., Zeng, G.M., Gong, J.L., Liang, J., Xu, P., Zhang, C., Huang, B. Bin, 2014. Impact of humic/fulvic acid on the removal of heavy metals from aqueous solutions using nanomaterials: A review. Sci. Total Environ. 468–469, 1014–1027. https://doi.org/10.1016/j.scitotenv.2013.09.044

US EPA, 2000. Environmental Protection Agency, Environmental Response Team. Standard operating procedures – SOP 1–4.

Uyguner, C.S., Bekbolet, M., 2005. Evaluation of humic acid photocatalytic degradation by UV-vis and fluorescence spectroscopy. Catal. Today 101, 267–274. https://doi.org/10.1016/j.cattod.2005.03.011

Weiner, B., Poerschmann, J., Wedwitschka, H., Koehler, R., Kopinke, F.D., 2014. Influence of Process Water Reuse on Hydrothermal Carbonization of Paper. Sustain. Chem. Eng. 2, 2165–2171. https://doi.org/10.1021/sc500348v

Yang, F., Zhang, S., Cheng, K., Antonietti, M., 2019. A hydrothermal process to turn waste biomass into artificial fulvic and humic acids for soil remediation. Sci. Total Environ. 686, 1140–1151. https://doi.org/10.1016/j.scitotenv.2019.06.045

Yang, X., Tsibart, A., Nam, H., Hur, J., El-Naggar, A., Tack, F.M.G., Wang, C.H., Lee, Y.H., Tsang, D.C.W., Ok, Y.S., 2019. Effect of gasification biochar application on soil quality: Trace metal behavior, microbial community, and soil dissolved organic matter. J. Hazard. Mater. 365, 684–694. https://doi.org/10.1016/j.jhazmat.2018.11.042

Yuan, D.H., Guo, X.J., Wen, L., He, L.S., Wang, J.G., Li, J.Q., 2015. Detection of Copper (II) and Cadmium (II) binding to dissolved organic matter from

761 macrophyte decomposition by fluorescence excitation-emission matrix spectra
762 combined with parallel factor analysis. Environ. Pollut. 204, 152–160.
763 https://doi.org/10.1016/j.envpol.2015.04.030

764 Zherebtsov, S.I., Malyshenko, N. V., Bryukhovetskaya, L. V., Lyrshchikov, S.Y.,
765 Ismagilov, Z.R., 2015. Sorption of copper cations from aqueous solutions by
766 brown coals and humic acids. Solid Fuel Chem. 49, 294–303.
767 https://doi.org/10.3103/S0361521915050110

768

769

770

Table 1. Biomass, additives, temperature, and reaction time used for hydrothermal carbonization and recarbonization.

Carbonization/ Recarbonization	**Reaction**	**Biomass**	**Additive (4% v/v)**	**Temp.**	**Time**
HH_3PO_4	1	Vinasse Sugarcane bagasse	Phosphoric Acid	230 °C	13 h
HH_2SO_4	2	Vinasse Sugarcane bagasse	Sulfuric Acid	230 °C	13 h
RHH_3PO_4	3	Process water (from reaction1) Sugarcane bagasse	Phosphoric Acid	230 °C	13 h
RHH_2SO_4	4	Process water (from reaction 2) Sugarcane bagasse	Sulfuric Acid	230 °C	13 h

Table 2
Click here to download Table: Table 2.doc

Table 2. Carbon (C), hydrogen (H), nitrogen (N), oxygen (O) and sulfur (S) contents; O/C, H/C, and C/N atomic ratios; and absorbance ratios E_{465}/E_{665} and E_{270}/E_{407} for HA and HLA samples.

HA/HLA	C (%)	H (%)	N (%)	O (%)	S (%)	O/C	H/C	C/N	E_{465}/E_{665}	E_{270}/E_{407}
TM I*	51.24	3.80	3.41	40.61	0.94	0.59	0.89	17.80	3.92	2.81
TM II*	39.62	4.05	4.04	51.37	0.92	0.97	1.23	11.38	4.33	3.43
TM III*	50.22	3.69	2.97	42.14	0.98	0.63	0.88	19.95	4.18	2.90
HH_2SO_{4}**	51.95	5.25	1.47	39.88	1.45	0.57	1.21	43.30	5.71	4.06
HH_3PO_{4}**	62.27	5.62	2.60	28.47	1.04	0.34	1.08	28.83	5.33	3.93
RHH_2SO_{4}**	48.90	4.46	1.20	37.99	7.45	0.58	1.09	51.00	3.50	3.33
RHH_3PO_{4}**	53.54	4.82	1.83	35.92	0.89	0.50	1.08	34.31	4.67	3.19

* natural humic acids; ** humic-like acids

Table 3
Click here to download Table: Table 3.doc

Table 3. Relative value (% of total area) and indexes obtained from ^{13}C-CPMAS- NMR spectra of HA and HLA samples.

	^{13}C NMR region (ppm)							^{13} C NMR indexes		
HA/HLA	**220-190**	**190-160**	**160-145**	**145-110**	**110-60**	**60-45**	**45-0**	**ARM**	**A/OA**	**HB/HI**
TM I*	4.93	15.41	5.86	34.98	17.87	5.55	15.41	1.23	0.86	1.45
TM II$^{\#}$	-	-	-	-	-	-	-	-	-	-
TM III*	6.43	14.11	4.98	30.08	17.22	6.43	20.75	0.92	1.20	1.48
HH_2SO_4**	1.75	6.11	6.55	33.62	3.06	5.24	43.67	0.86	14.29	5.19
HH_3PO_4**	2.55	2.55	3.57	29.59	1.02	9.69	51.02	0.64	50.00	5.32
RHH_2SO_4**	3.03	5.30	7.95	42.80	2.65	0.38	37.88	1.25	14.29	7.80
RHH_3PO_4**	1.79	1.79	8.04	36.16	0.45	7.14	44.64	0.98	100.00	7.96

* natural humic acids; ** humic-like acids; $^{\#}$ not realized / ARM = aromaticity index [(110 − 160) / Σ (0 − 45) + (60 − 110)]; A/OA = alkyl/O-alkyl index (0 − 45) / (60 − 110); HB/HI = hydrophobicity index = [Σ (0 − 45) + (110–160) / Σ (45 − 60) + (60 − 110) + (160 − 190)].

Table 4
Click here to download Table: Table 4.doc

Table 4. Log K, CL, CC, and bias values for components 1 and 2 regarding the interaction of HA and HLA with Cu(II) ions.

HA/HLA	Component 1				Component 2			
	Bias	CL (mol L^{-1})	Log K	CC (mmol of Cu g^{-1} C)	Bias	CL (mol L^{-1})	Log K	CC (mmol of Cu g^{-1} C)
TM I*	2.25	6.50E-06	5.36	1.27	4.18	3.50E-06	5.58	0.68
TM II*	0.96	6.70E-06	5.41	1.69	2.18	3.20E-06	5.60	0.81
TM III*	1.98	8.00E-06	5.30	1.59	2.29	4.50E-06	5.59	0.90
HH_2SO_4**	2.04	2.40E-05	4.89	4.62	2.67	1.00E-05	5.09	1.92
HH_3PO_4**	0.47	2.40E-05	4.88	3.85	0.49	1.70E-05	5.06	2.73
RHH_2SO_4**	0.71	3.20E-05	4.89	6.54	0.77	2.50E-05	5.08	5.11
RHH_3PO_4**	0.27	1.80E-05	4.90	3.36	0.35	1.40E-05	5.09	2.61

* natural humic acids; ** humic-like acids

Figure 1
Click here to download Figure: Figure 1.doc

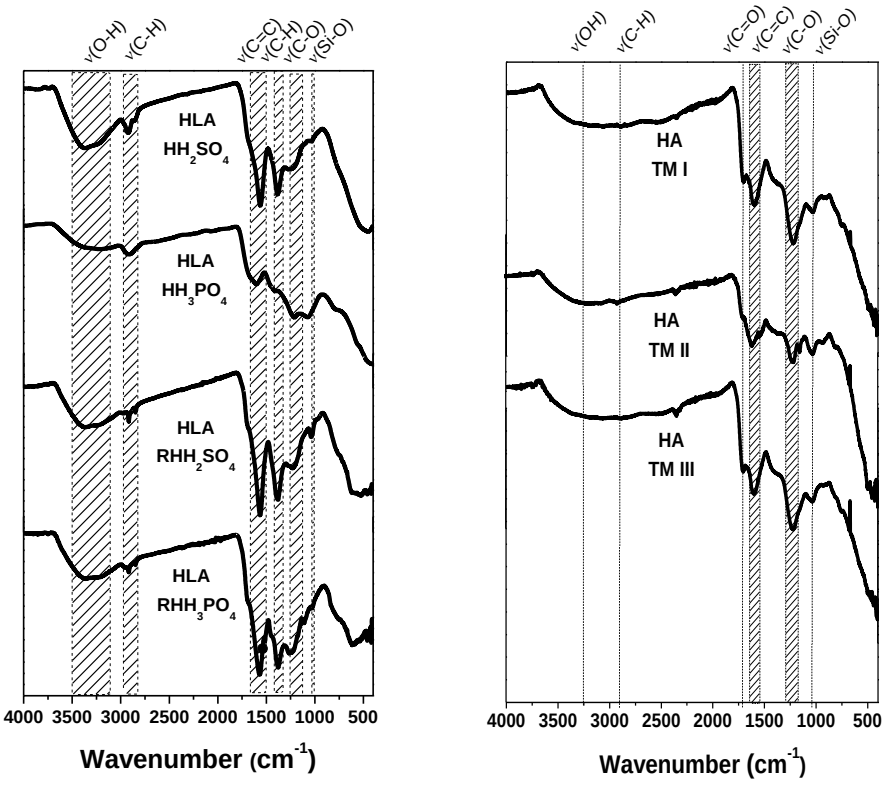

Fig.1. FTIR spectra for HLA isolated from hydrochar (a) and HA isolated from soil (b).

Figure 2
Click here to download Figure: Figure 2.doc

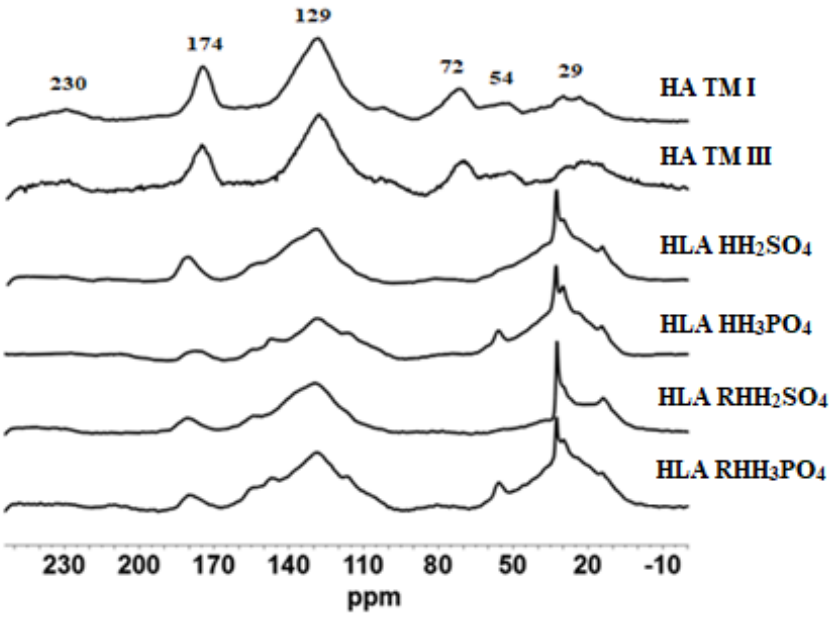

Fig.2. Solid-state ^{13}C NMR spectra of HA and HLA.

Figure 3
Click here to download Figure: Figure 3.doc

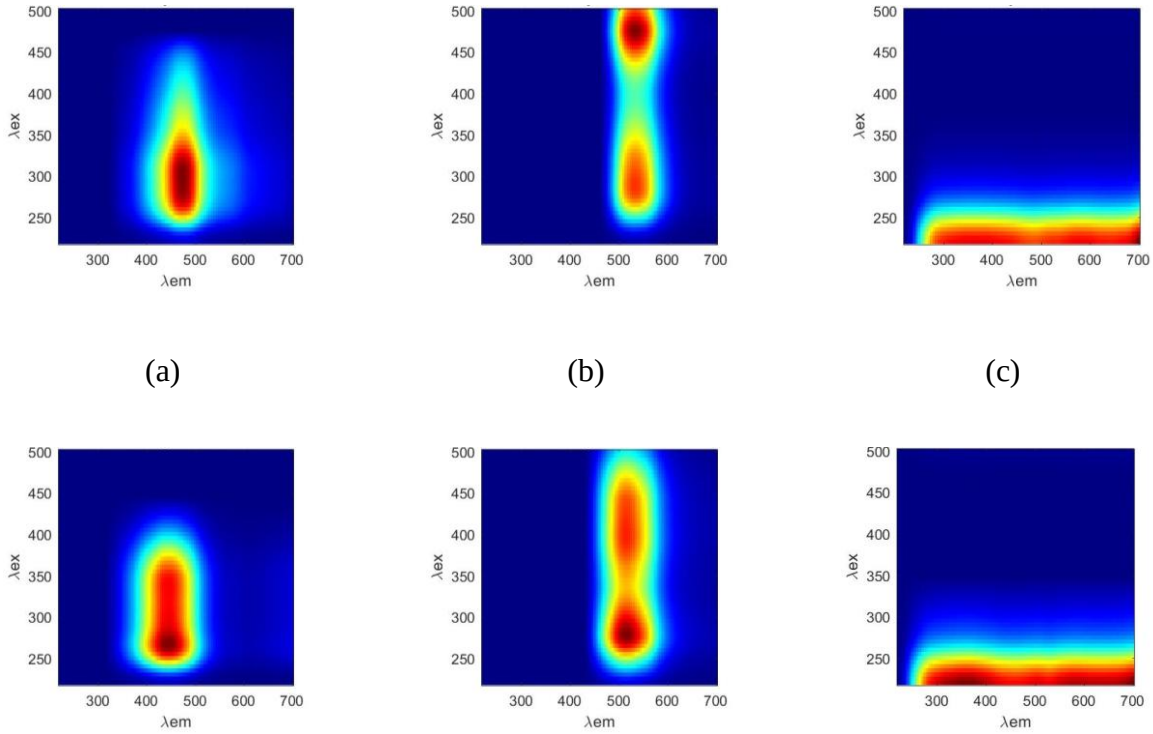

(a) (b) (c)

(d) (e) (f)

Fig. 3. Components 1, 2, and 3 obtained by CP/PARAFAC for interaction of HA (a, b and c, respectively) and components 1, 2, and 3 for interaction of HLA (d, e and f, respectively) with Cu(II) ions.

Figure 4
Click here to download Figure: Figure 4.doc

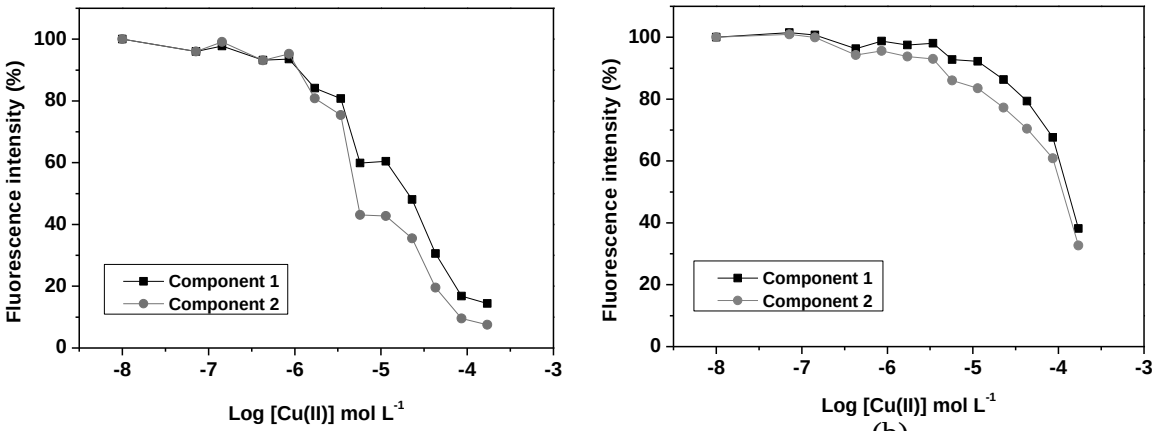

Fig. 4. Contribution of relative fluorescence intensity for components 1 and 2 regarding the interaction of TM I HA (a) and HH_2SO_4 HLA (b) with Cu (II) ions.

Figure 5
Click here to download Figure: Figure 5.doc

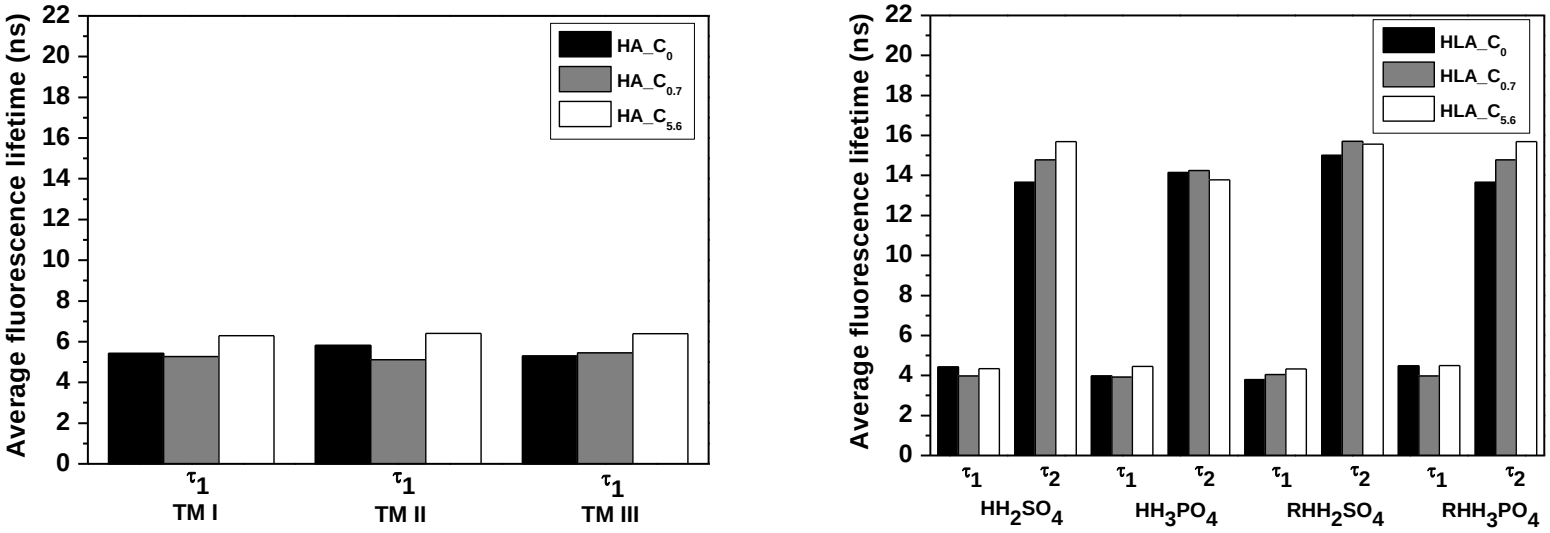

Fig. 5. Average fluorescence lifetime distribution for HA (τ_1) (a) and HLA (τ_1 and τ_2) (b) when interacting with Cu(II) ions at concentration: C_0 = no copper added, $C_{0.7}$ = 0.7 mg L^{-1} and $C_{5.6}$ = 5.6 mg L^{-1}.